

Singularity Analysis for Redundant Manipulators of Arbitrary Kinematic Structure

Ahmad A. Almarkhi^a and Anthony A. Maciejewski^b

Department of Electrical and Computer Engineering, Colorado State University, Fort Collins, CO 80523-1373, U.S.A.

Keywords: Redundant Robots, Singularities, Kinematics.

Abstract: This paper presents a technique to identify singularities of any rank for a robot of any kinematic structure. The technique is based on computing the gradient of singular values of the robot Jacobian. The algorithm deals with the situations when two or more singular values become nearly equal and their corresponding singular vectors are ill-defined. Also, an algorithm is developed to identify the physically meaningful singular directions from the high dimensional singular subspaces of high-rank singularities. The suggested technique is applied to a 4-DoF and a 7-DoF robot to show its efficacy at identifying robot singularities of all ranks and dealing with the ill-defined singular directions.


1 INTRODUCTION


A robot singular configuration is a configuration in which the robot's end effector loses the ability to move in one (or more) direction(s), i.e., singular direction(s). Such singular configurations are usually called *singularities* (Baker and Wampler, 1988). Robot singularities are also called *critical points* (Burdick, 1989) or *special configurations* (Hunt, 1986). At a singularity, there is no joint velocity that can result in an end-effector velocity in a singular direction(s). Singularities result from having the corresponding Jacobian (\mathbf{J}) columns be linearly dependent. The singular value decomposition (SVD) of \mathbf{J} can reveal immediate information about singularities. At a singularity, one (or more) singular value(s) of the robot Jacobian are zero. Robot singularities can offer mechanical advantages (Kieffer and Lenarcic, 1994), however, they require more sophisticated inverse kinematics solutions (Nakamura and Hanafusa, 1986).

Identifying robot singularities has been extensively studied. For non-redundant manipulators, where \mathbf{J} is square, singularities can be found by symbolically solving for conditions when the determinant of \mathbf{J} equals zero ($|\mathbf{J}| = 0$) (Waldron et al., 1985). For redundant manipulators, where $|\mathbf{J}|$ does not exist, the conditions that make $|\mathbf{J}\mathbf{J}^T| = 0$ can be computed,

but this is usually difficult to solve. In this case, one viable approach is to solve for conditions that make all the 6×6 sub-Jacobians singular, i.e., the determinants of all sub-Jacobians equal zero (Litvin et al., 1986), but this also becomes infeasible for robots with a large number of degrees of freedom (DoF). For example, an 8-DoF manipulator requires computing the determinants of 28 sub-Jacobians. In addition, these techniques typically lack the ability to provide information about the singular vector(s) associated with a singularity.

To more easily identify singularities and find singular directions, (Sugimoto et al., 1982) suggested using the fact that at a singularity, there must be a screw reciprocal to all screws that represent the columns of the robot Jacobian. This technique has been used to identify the rank-1 singularity conditions and the singular directions for 7-DoF manipulators (Boudreau and Podhorodeski, 2010). The reciprocity-based methodology has also been used to find the rank-1 singularities of an 8-DoF manipulator (Nokleby and Podhorodeski, 2004b). In addition, it was extended to identify the rank-2 singularities of a 7-DoF manipulator (Nokleby and Podhorodeski, 2004a). This technique shows its merit of being relatively easy and extendable, but it is highly dependent on selecting a reference frame that simplifies the computation of \mathbf{J} . Building on the reciprocity-based approach, researchers have suggested further simplifications of the Jacobian by performing elementary transformations on the Jacobian before solving

^a  <https://orcid.org/0000-0002-5767-6103>

^b  <https://orcid.org/0000-0002-1376-5825>

for the singularity conditions as in (Xu et al., 2013). This approach has been further employed in performing singularity avoidance for manipulators with non-spherical wrists (Xu et al., 2016). All these techniques work well for simple classes of kinematically redundant manipulators and for rank-1 singularities. Such manipulators have their successive joint axes either perpendicular or parallel, which makes computing \mathbf{J} relatively easy.

In this paper we suggest a technique to find the singularities of a manipulator with an arbitrary degree of redundancy and arbitrary kinematic structure. This can be achieved by driving a certain singular value, σ_i , of \mathbf{J} to zero by following the gradient descent of that singular value, i.e., $-\nabla\sigma_i$. The complexity of this technique is independent of the rank of the singularity. In addition, we present an algorithm to identify the singular directions at high-rank singularities.

The rest of this paper is organized as follows. Methodologies to identify robot singularities and their corresponding singular directions are presented in section 2. In section 3, the results of applying the methodologies to a 4-DoF robot and a 7-DoF robot are discussed. Finally, the conclusions of this work are presented in section 4.

2 SINGULARITY ANALYSIS

2.1 Background

The forward kinematics of an n -DoF robot that is acting in an m -dimensional workspace can be written as

$$\dot{\mathbf{x}} = \mathbf{J}\dot{\boldsymbol{\theta}} \quad (1)$$

where $\dot{\mathbf{x}}$ is an $m \times 1$ vector representing the end-effector velocity, \mathbf{J} is the $m \times n$ robot Jacobian, and $\dot{\boldsymbol{\theta}}$ is an $n \times 1$ vector that represents the joint angle rates. For redundant robots, $n > m$, where $n - m$ is the degree of redundancy. For a redundant manipulator, \mathbf{J} is not a square matrix, and thus not invertible, however, an inverse kinematics solution can be found using

$$\dot{\boldsymbol{\theta}} = \mathbf{J}^+ \dot{\mathbf{x}} + \mathbf{n}_J \quad (2)$$

where \mathbf{J}^+ is the pseudoinverse of \mathbf{J} and \mathbf{n}_J is an arbitrary vector in the null space of the Jacobian.

The singular value decomposition of \mathbf{J} can be represented as

$$\mathbf{J} = \sum_{i=1}^r \sigma_i \mathbf{u}_i \mathbf{v}_i^\top \quad (3)$$

where r is the rank of \mathbf{J} , the σ_i 's are the ordered singular values, i.e., $\sigma_1 \geq \sigma_2 \geq \dots \geq \sigma_m \geq 0$, the unit vectors \mathbf{u}_i represent the output singular vectors, and

\mathbf{v}_i are the input singular vectors. For a robot at a rank- n singularity, there are n singular values, σ_i 's, that become zero. Thus, employing a technique that minimizes singular values of \mathbf{J} can be used to identify robot singular configurations.

2.2 Identifying Robot Singularities

In this section, we explain how to employ the gradient descent of a singular value of \mathbf{J} to drive a robot of an arbitrary kinematic structure to a singularity. This technique is not limited by the rank of the singularity. The singular value σ_i in (3) can be expressed as

$$\sigma_i = \mathbf{u}_i^\top \mathbf{J} \mathbf{v}_i. \quad (4)$$

Differentiating (4) with respect to time results in

$$\dot{\sigma}_i = \dot{\mathbf{u}}_i^\top \mathbf{J} \mathbf{v}_i + \mathbf{u}_i^\top \dot{\mathbf{J}} \mathbf{v}_i + \mathbf{u}_i^\top \mathbf{J} \dot{\mathbf{v}}_i. \quad (5)$$

One can note that $\mathbf{u}_i^\top \mathbf{u}_j$ and $\mathbf{v}_i^\top \mathbf{v}_j$ are zero for $i \neq j$ and that the derivative of a unit vector is orthogonal to that vector. So, (5) can be further simplified to (Maciejewski, 1988)

$$\dot{\sigma}_i = \mathbf{u}_i^\top \dot{\mathbf{J}} \mathbf{v}_i. \quad (6)$$

The partial derivative of σ_i with respect to some θ_k can be expressed as

$$\frac{\partial \sigma_i}{\partial \theta_k} = \mathbf{u}_i^\top \frac{\partial \mathbf{J}}{\partial \theta_k} \mathbf{v}_i \quad (7)$$

where

$$\frac{\partial \mathbf{J}}{\partial \theta_k} = \begin{bmatrix} \frac{\partial j_1}{\partial \theta_k} & \frac{\partial j_2}{\partial \theta_k} & \dots & \frac{\partial j_n}{\partial \theta_k} \end{bmatrix}. \quad (8)$$

The partial derivative of the i^{th} column of the Jacobian is given by (Klein and Chu, 1997), (Groom et al., 1999)

$$\frac{\partial \mathbf{j}_i}{\partial \theta_k} = \begin{cases} \begin{bmatrix} (\mathbf{z}_k^\top \mathbf{p}_i) \mathbf{z}_i - (\mathbf{z}_k^\top \mathbf{z}_i) \mathbf{p}_k \\ \mathbf{z}_k \times \mathbf{z}_i \end{bmatrix}, & k < i \\ \begin{bmatrix} (\mathbf{z}_i^\top \mathbf{p}_k) \mathbf{z}_k - (\mathbf{z}_i^\top \mathbf{z}_i) \mathbf{p}_k \\ \mathbf{0} \end{bmatrix}, & k \geq i \end{cases} \quad (9)$$

Then, the gradient of σ_i for any \mathbf{J} can be simply computed from (7), (8), and (9), as

$$\nabla \sigma_i = \left[\frac{\partial \sigma_i}{\partial \theta_1}, \frac{\partial \sigma_i}{\partial \theta_2}, \dots, \frac{\partial \sigma_i}{\partial \theta_n} \right]. \quad (10)$$

Now that one can compute $\nabla \sigma_i$, it is possible to employ the gradient descent technique to locate a minima for any singular value σ_i . In the following, we explain an algorithm to find rank-1 and higher rank singularities.

2.2.1 Identifying Rank-1 Singularities

For rank-1 singularities, one can employ the general equation

$$\boldsymbol{\theta}^{(k+1)} = \boldsymbol{\theta}^{(k)} - \alpha_k \nabla \sigma_i^{(k)} \quad (11)$$

where, $\boldsymbol{\theta}^{(k+1)}$ is a vector that represents the new joint angles of a robot, the vector $\boldsymbol{\theta}^{(k)}$ is the current joint angles, α_k is an adaptive step size, and $\nabla \sigma_i^{(k)}$ is the gradient of σ_i ($\sigma_i = \sigma_m$ for rank-1 singularities). In order to identify all rank-1 robot singular configurations, one can start by generating random configurations that span the robot joint space. Then, from each random configuration, one can move the robot along the gradient descent of σ_m as in (11). For faster convergence to a singularity, one can use the steepest descent method, in which α_k needs to be adaptive, i.e., it is chosen at each iteration to achieve a maximum decrease in σ_m . This can be done by conducting a one-dimensional search along the $-\nabla \sigma_m^{(k)}$ direction until a minimizer, $\boldsymbol{\theta}^{(k+1)}$, is found.

2.2.2 Identifying Rank-2 Singularities

A robot is said to be in a rank-2 singularity if $\epsilon > \sigma_{m-1} \geq \sigma_m$, where ϵ is a small threshold (virtually zero). To identify rank-2 singularities, one can start with a population of random joint configurations and employ (11) by moving along the $-\nabla \sigma_{m-1}^{(k)}$ direction until the $\sigma_{m-1} < \epsilon$ condition is satisfied. However, it is not uncommon for an undesirable behavior to occur, that results from having the two singular values σ_{m-1} and σ_m become nearly equal before they reach zero, i.e., $\sigma_{m-1} \approx \sigma_m > \epsilon$. In this case, the two singular values are not distinct, which means that their corresponding singular vectors are ill-defined. In other words, any singular vectors (\mathbf{u} and \mathbf{v}) in the $\{\mathbf{u}_{m-1}, \mathbf{u}_m\}$ and $\{\mathbf{v}_{m-1}, \mathbf{v}_m\}$ subspaces are valid for solving (6). Figure 1, shows the behavior of the algorithm when the two smaller singular values become nearly equal through the process of driving a robot into a rank-2 singularity. In this case, $\sigma_5 \approx \sigma_6$ (at around iteration 600), which makes them indistinct and their corresponding singular vectors ill-defined. The direction of $\nabla \sigma_5$ can completely change direction from one iteration to another, which affects the rate of convergence.

To overcome this unwanted effect, one can start with moving the robot along the $-\nabla \sigma_{m-1}^{(k)}$ direction until σ_5 and σ_6 become very close in value. Then, a combination between the two gradients is computed. Because the singular value decomposition is not unique in these cases, any singular vectors \mathbf{u} and \mathbf{v} in the subspace associated with the equal singular

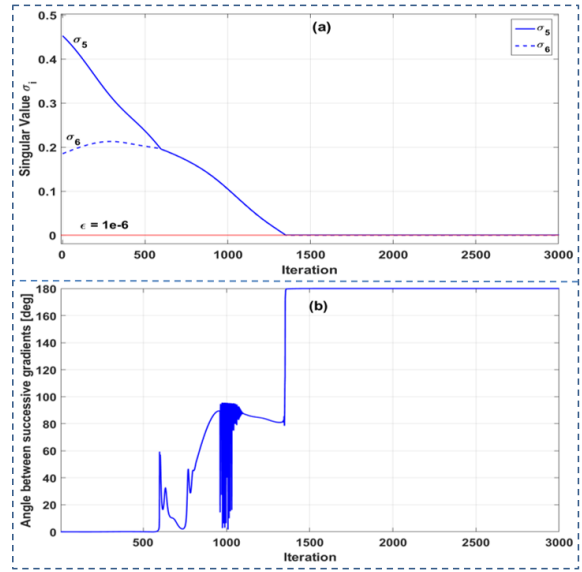


Figure 1: In subplot (a), the evolution of σ_5 and σ_6 is shown as the standard gradient descent algorithm is employed. The singular value σ_5 is minimized until $\sigma_5 \approx \sigma_6$ at around iteration 600. When they become nearly equal, the angle between the gradients in successive iterations becomes large. These angles are plotted in (b), where the change in the angles reaches 180° . It is clear that the convergence requires a long time (about 3000 iterations) due to the large change in the gradient direction. In this case, the convergence time is approximately 40 seconds. The threshold, $\epsilon = 10^{-6}$, is indicated with a red horizontal line.

values are valid. One can rotate the singular subspace such that the angle between $\nabla \sigma_5^{(k)}$ and $\nabla \sigma_6^{(k)}$ is minimized, i.e.,

$$\begin{aligned} \mathbf{u}_{5(new)} &= \mathbf{u}_5 \cos \phi + \mathbf{u}_6 \sin \phi \\ \mathbf{u}_{6(new)} &= \mathbf{u}_6 \cos \phi - \mathbf{u}_5 \sin \phi \\ \mathbf{v}_{5(new)} &= \mathbf{v}_5 \cos \phi + \mathbf{v}_6 \sin \phi \\ \mathbf{v}_{6(new)} &= \mathbf{v}_6 \cos \phi - \mathbf{v}_5 \sin \phi \end{aligned} \quad (12)$$

where ϕ is the angle of rotation. It should be noted that the angle between the gradients of σ_5 and σ_6 can vary from 0 to π based on the angle of rotation ϕ . A suitable selection of the rotation angle for the singular subspaces is crucial in minimizing the change in the gradient direction from one iteration to another. Once the $\nabla \sigma_5^{(k)}$ and $\nabla \sigma_6^{(k)}$ that have the minimum angle between them are computed, a combination that minimizes σ_5 can be found

$$\nabla \sigma^{(k)} = \gamma \nabla \sigma_5^{(k)} + (1 - \gamma) \nabla \sigma_6^{(k)} \quad (13)$$

where $\nabla \sigma^{(k)}$ is the desired gradient and γ is a positive scalar where $0 \leq \gamma \leq 1$. This linear search will minimize the change in the gradient direction from one iteration to another. After $\nabla \sigma^{(k)}$ is computed, the

steepest descent method is applied to find an optimal value of α_k in (11) that minimizes σ_5 . An analogous process can be employed for identifying higher rank singularities.

2.2.3 Identifying High-rank Singularities

To identify high-rank singularities, i.e., where three or more singular values become zero, one can employ a similar approach to that applied for identifying rank-2 singularities. For a robot in a singular configuration, \mathbf{J} is of rank r if $\sigma_i = 0$ for $i > r$, which also means the robot is in a rank- $(m - r)$ singularity. To find high-rank singularities, one can move the robot by iteratively solving (11) until a desired σ_i reaches zero. While moving along the $-\nabla\sigma_i$ direction, it is possible that σ_i and σ_{i+1} become nearly equal. In this case, the procedure in the previous section can be applied.

In some cases, more than two singular values become nearly equal but larger than the threshold, i.e., $\sigma_i \approx \sigma_{i+1} \approx \dots \approx \sigma_m > \varepsilon$. For the purpose of illustration, we will consider the case where a robot is being driven to a rank-3 singularity when the situation $\sigma_4 \approx \sigma_5 \approx \sigma_6 > \varepsilon$ occurs, as illustrated in Figure 2. One can note that around iteration 186 in Figure 2 all three singular values became very close in value. At this point, the angle between the gradient of σ_4 in successive iterations (the angles between $\nabla\sigma_4^{(k-1)}$ and $\nabla\sigma_4^{(k)}$) became 170° , which resulted from having the singular values indistinct and their corresponding singular vectors ill-defined. This also contributed to an unwanted increase in σ_4 because the gradients switched direction. In this case, one can rotate their corresponding singular subspaces to find a suitable rotation that minimizes the sum of the angles between the three gradients. The solution is to minimize an objective function H , where

$$H = \sum_{(i=r+1)}^m \sum_{(j=i+1)}^m \theta_{i,j} \quad (14)$$

and $\theta_{i,j}$ is the angle between $\nabla\sigma_i$ and $\nabla\sigma_j$. The rotation of the singular subspaces can be done by iteratively employing (12). That is, because the singular subspaces are three-dimensional (or higher), one can iteratively rotate one plane at a time, i.e., in this case, $\{\mathbf{u}_4, \mathbf{u}_5\}$ and $\{\mathbf{v}_4, \mathbf{v}_5\}$, then $\{\mathbf{u}_5, \mathbf{u}_6\}$ and $\{\mathbf{v}_5, \mathbf{v}_6\}$, and so on. This iterative rotation should be done until the sum of the angles between all gradients is minimized. After finding the gradients of the singular values, one can use (13) to compute a combination between the first two gradients, $\nabla\sigma_4$ and $\nabla\sigma_5$, that minimize σ_4 . Then, using (13) again to compute a combination between the resulting gradient and $\nabla\sigma_6$ that

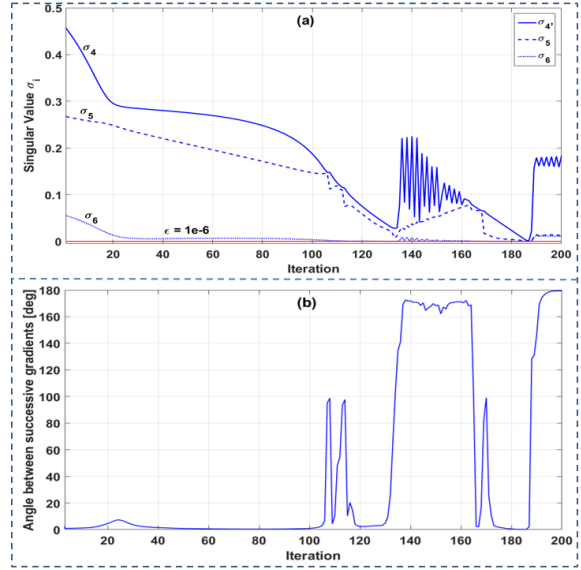


Figure 2: In (a), the singular value σ_4 is minimized until iteration 106, where ($\sigma_4 \approx \sigma_5$). At iterations 135 and 186 the singular values σ_4 , σ_5 , and σ_6 become nearly equal. Subfigure (b) shows the change in the angle between the gradients in successive iterations. The change of angle reaches 170° when the three singular values become nearly equal. In this case, the singular values σ_4 , σ_5 , and σ_6 never converge to zero. The threshold, $\varepsilon = 10^{-6}$, is indicated with a red horizontal line.

minimizes σ_4 . This approach guarantees achieving a minimum amount of gradient direction change and thus a shorter convergence time.

This process can continue until the algorithm cannot converge to any higher rank singularities. This algorithm, along with an adaptive step size, was applied to the same robot that resulted in Figure 2 and the results are shown in Figure 3. It is clear that the convergence is faster and the change in the gradient angle is smaller. The average convergence time was improved from 40 seconds to less than 2 seconds when the proposed technique is employed.

If one applies the above algorithm to an initial population of random configurations then one can identify all the singular configurations of various ranks. It is then possible to analyze the resulting singularities to determine the singularity conditions for the robot. Some singularity conditions depend on the values of a few joints while other joints can take any value. One may observe that a singularity can be satisfied by an infinite number of joint configurations. In the next section, we discuss a mathematical approach to identify singular directions associated with the singularities that are physically meaningful.

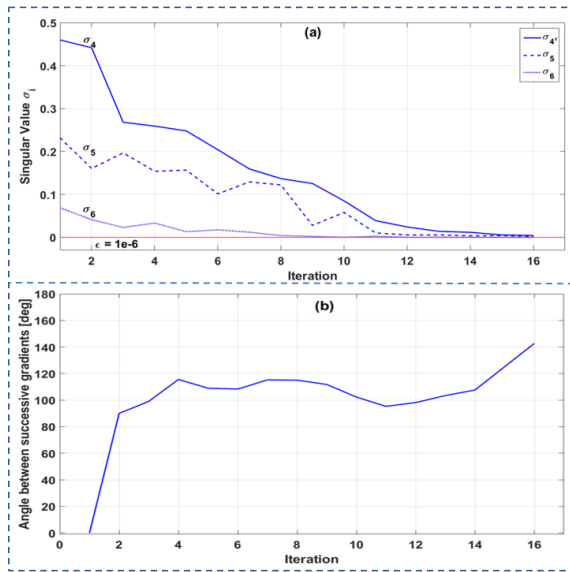


Figure 3: This figure shows the behavior of the singular values when the proposed algorithm is applied to a robot to find a rank-3 singularity. This is the same robot as shown in Figure 2. Subfigure (a) shows the values of the three smaller singular values, σ_4 , σ_5 , and σ_6 , while applying the algorithm with an adaptive step size α_k . In subfigure (b), the angles between the gradients in successive iterations are shown. The angles average around 120° . The algorithm converges in 16 iterations. The convergence time in this case is less than two seconds. The threshold, $\epsilon = 10^{-6}$, is indicated with a red horizontal line.

2.3 Identifying Singular Directions

For a robot Jacobian \mathbf{J} with rank r , the last $m - r$ output singular vectors, i.e., \mathbf{u}_i 's, span the directions of lost end-effector motion. For spatial manipulators, these singular vectors are 6-dimensional and represent a simultaneous translational and rotational velocity. For rank-1 singularities, there is only one unique singular direction, \mathbf{u}_m , and it is easy to visualize. At higher rank singularities, the singular value decomposition is not unique. Thus, the singular vectors corresponding to the zero singular values ($\sigma_{r+1}, \sigma_{r+2}, \dots, \sigma_m$) are ill defined and will likely not be well aligned with the world (or task) frame of the robot. However, one can apply Givens rotations to these vectors in order to identify an intuitive representation for the lost end effector motion. Consider Figure 4, that shows a 7-DoF robot in a rank-3 singularity, where both subfigures correspond to the same robot in the same singular configuration. The original singular vectors, identified by employing the singular value decomposition, can be rotated to a more

¹Figure 4, 6, 7, 8, and 9 are produced using the Robotics Toolbox (Corke, 2017).

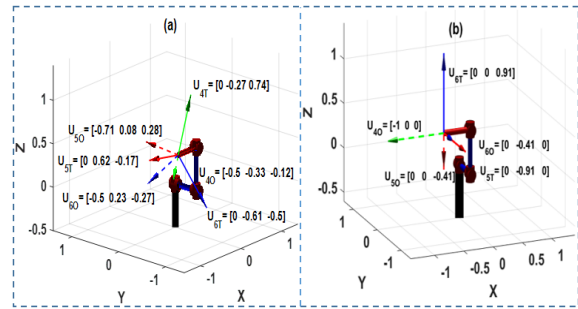


Figure 4: A 7-DoF robot in the same rank-3 singularity is presented.¹In subfigure (a), the three SVD-generated singular directions are indicated. In subfigure (b), the singular directions are plotted after they are properly rotated. The singular directions, \mathbf{u}_4 , \mathbf{u}_5 , and \mathbf{u}_6 are represented by green, red, and blue respectively. Dotted arrows represent rotational velocity and solid arrows represent translational velocity.

intuitive set that is aligned with the world coordinate frame as follows:

$$[\mathbf{u}_4 \mathbf{u}_5 \mathbf{u}_6] = \begin{bmatrix} 0 & 0 & 0 \\ -0.27 & 0.62 & -0.61 \\ 0.74 & -0.17 & -0.50 \\ -0.50 & -0.71 & -0.50 \\ -0.33 & 0.08 & 0.23 \\ -0.12 & 0.28 & -0.27 \end{bmatrix} \Rightarrow \begin{bmatrix} 0 & 0 & 0 \\ 0 & -0.91 & 0 \\ 0 & 0 & 0.91 \\ -1 & 0 & 0 \\ 0 & 0 & -0.41 \\ 0 & -0.41 & 0 \end{bmatrix}$$

Using the rotated subspace above (shown in Figure 4(b)), one can easily determine that there is no joint velocity that can generate any rotational velocity around the $-X$ direction (green). In addition, the robot cannot have a simultaneous velocity with the illustrated components of $-Y$ translational motion with $-Z$ rotational motion (red). Likewise, there are no joint rates that can generate a simultaneous velocity with the illustrated components of Y translational motion with $-Z$ rotational motion (blue). In the next section, we illustrate the results of applying the proposed algorithms to robots of different kinematic structures.

3 CASE STUDIES

3.1 Introduction

Our algorithm to identify robot singularities is neither limited by the kinematic structure of the robot, nor by the rank of the singularity. We employed it on several 4-DoF regional and 7-DoF spatial robots and present the results of one 4-DoF and one 7-DoF robot here. For each robot we start with 10,000 random configurations in the joint space. From each point, we apply the gradient-based algorithm to find rank-1 and all higher rank singularities. The resulting singular

vectors are then rotated to the most intuitive representation of the lost directions of motion.

3.2 4-DoF Regional Robot

We study a locally optimal fault-tolerant 4-DoF robot presented in (Ben-Gharbia et al., 2013) with the DH parameters given in Table 1. This robot is a spatial positioning (regional) manipulator, i.e., it has a 3-dimensional workspace. Our focus is on identifying the singular configurations of this manipulator.

Table 1: DH parameters of an example 4-DoF manipulator.

$Link_i$	α_i [radians]	a_i [m]	d_i [m]	θ_i [radians]
1	$\pi/2$	$\sqrt{2}$	0	θ_1
2	$-\pi/2$	$\sqrt{2}$	1	θ_2
3	$\pi/2$	$\sqrt{2}$	-1	θ_3
4	0	$\sqrt{3}/2$	1/2	θ_4

It was found that this robot has only rank-1 singularities as presented in Figure 5. These singularities are arranged along continuous manifolds in the joint space. This means that the robot can continuously move while staying in a singular configuration. Note that these are not the same as the self-motion manifolds.

Because the robot does not have any high-rank singularities, the presentation of the singular directions is straightforward. The singular direction, \mathbf{u}_3 , gives the actual direction of the loss of the end-effector velocity. Figure 6 shows the 4-DoF robot in two different rank-1 singularities along with the singular directions with respect to the world frame.

3.3 Mitsubishi PA-10 Robot

3.3.1 Introduction

The Mitsubishi PA-10 is a 7-DoF manipulator with a 6-dimensional work space. Its kinematic structure is similar to the human arm with three spherical joints in the shoulder, one joint in the elbow, and three spherical joints in the wrist. The DH parameters of the PA-10 are listed in Table 2. The singularity analysis on the PA-10 resulted in rank-1, rank-2, and rank-3 singularities being identified. We were able to find singularity conditions for each singularity rank. The singular directions, \mathbf{u}_i 's, were also identified and appropriately rotated. In all figures, loss of directional velocity is indicated with a solid arrow, while the loss of rotational velocity is indicated with a dotted arrow. Blue arrows indicate \mathbf{u}_6 , red arrows indicate \mathbf{u}_5 , and green arrows indicate \mathbf{u}_4 .

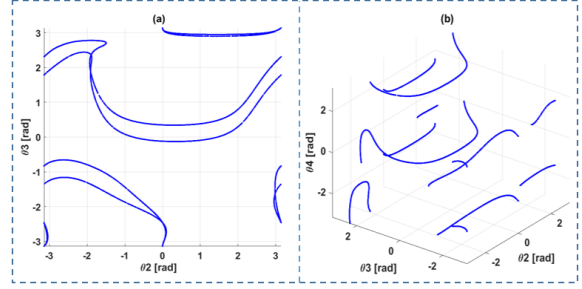


Figure 5: This figure illustrates the 4-DoF robot rank-1 singularities. In (a) the singular configurations are shown using a 2-D projection in $[\theta_2, \theta_3]$. In (b) a 3-D projection in $[\theta_2, \theta_3, \theta_4]$ is shown.

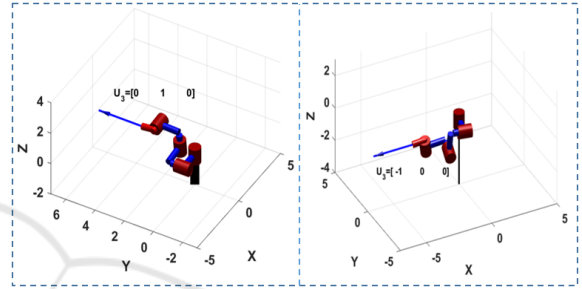


Figure 6: This figure shows the 4-DoF robot in two different rank-1 singular configurations. In (a) the robot is shown in the configuration $\theta = [-3.11, 3.02, -1.53, 0.15]$ rad. The singular direction corresponding to the singularity is $\mathbf{u}_3 = [0, 1, 0]^T$, which indicates that the singular direction is aligned with the Y direction. In (b) the robot is shown in the configuration $\theta = [-1.76, -1.85, -1.39, 0.02]$ rad. The singular direction is $\mathbf{u}_3 = [-1, 0, 0]^T$, which indicates that the singular direction is aligned with the $-X$ direction.

Table 2: DH parameters of the PA-10 robot.

$Link_i$	α_i [radians]	a_i [m]	d_i [m]	θ_i [radians]
1	$-\pi/2$	0	0	θ_1
2	$\pi/2$	0	0	θ_2
3	$-\pi/2$	0	0.45	θ_3
4	$\pi/2$	0	0	θ_4
5	$-\pi/2$	0	0.50	θ_5
6	$\pi/2$	0	0	θ_6
7	0	0	0.45	θ_7

3.3.2 Rank-1 Singularities

All rank-1 singularities are summarized in Table 3. Joint 4 is critical in that the robot will be singular if θ_4 is equal to $\pm\pi$ or 0. One can observe that joint 4 is the only joint that can change the distance between the shoulder and the wrist.

The robot singular directions that indicate the loss of the end-effector velocity are all shown in Figure 7. Because these are rank-1 singularities, their corresponding singular directions are well defined.

Table 3: PA-10 robot's rank-1 singular configurations².

i	θ_1	θ_2	θ_3	θ_4	θ_5	θ_6	θ_7
1	x	$\pm\pi, 0$	$\pm\pi/2$	x	x	x	x
2	x	$\pm\pi, 0$	x	x	x	$\pm\pi, 0$	x
3	x	x	x	$\pm\pi, 0$	x	x	x
4	x	x	x	x	$\pm\pi/2$	$\pm\pi, 0$	x

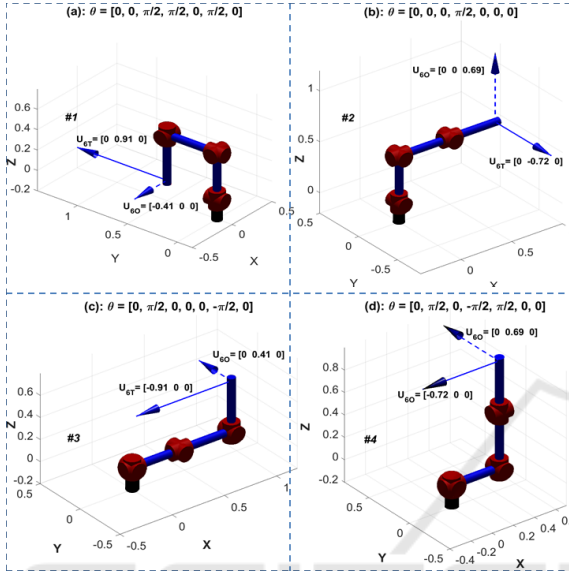


Figure 7: The PA-10 robot is shown in rank-1 singular configurations. The singular direction, u_6 , is also plotted for each singularity. The singularity conditions, 1, 2, 3, and 4, in Table 3 are satisfied in subfigures (a), (b), (c), and (d), respectively.

3.3.3 Rank-2 Singularities

The PA-10's rank-2 singularity conditions are shown in Table 4. The common feature between these conditions is that they do not depend on the value of θ_1 or θ_7 . We employed Givens rotation to make sure that the two singular vectors, u_5 and u_6 , are rotated to represent the most intuitive set of singular directions. Figure 8 shows the four singular conditions listed in Table 4.

3.3.4 Rank-3 Singularities

It was found that the PA-10 robot can have rank-3 singularities by aligning the axes of joints 1, 3, 5, and 7 so that their columns of the Jacobian are linearly dependent. The conditions for these rank-3 singularity configurations are listed in Table 5. As before, we have used Givens rotations to make the singular vectors, u_4 , u_5 , u_6 as intuitive as possible. Figure 9 shows the manipulator in two different rank-3 singularities.

²In all tables, "x" means the angle value does not matter.

Table 4: PA-10 robot's rank-2 singular configurations.

i	θ_1	θ_2	θ_3	θ_4	θ_5	θ_6	θ_7
1	x	$\pm\pi, 0$	$\pm\pi, 0$	$\pm\pi, 0$	x	x	x
2	x	$\pm\pi, 0$	x	$\pm\pi, 0$	x	$\pm\pi, 0$	x
3	x	x	x	$\pm\pi, 0$	$\pm\pi, 0$	$\pm\pi, 0$	x
4	x	$\pm\pi, 0$	$\pm\pi/2$	x	$\pm\pi/2$	$\pm\pi, 0$	x

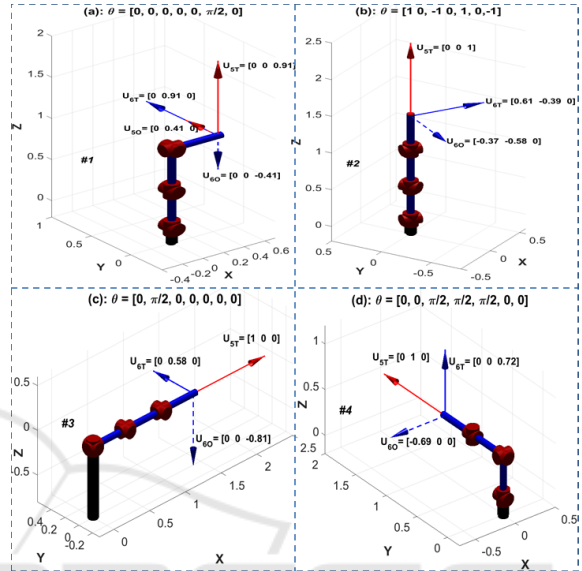


Figure 8: The PA-10 robot is shown in rank-2 singular configurations. The singular directions u_5 and u_6 are plotted for each singularity condition. The singularity conditions, 1, 2, 3, and 4, in Table 4 are represented in the subfigures (a), (b), (c), and (d), respectively.

lar configurations. One can observe that the rank-3 singularities occur for the PA-10 when it is completely stretched out (workspace boundary singularity) or when it is folded back on itself.

In general, our approach for identifying robot singularities does not consider physical joint limits. One

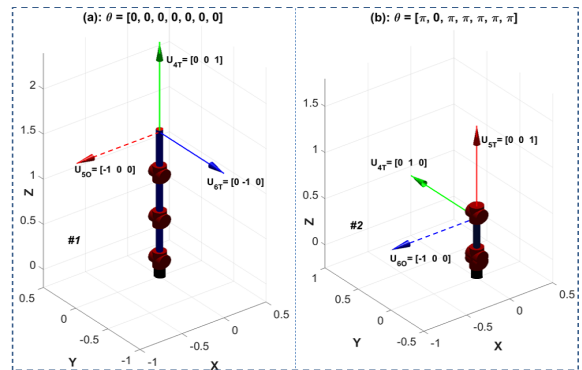


Figure 9: The PA-10 robot is shown in rank-3 singular configurations. The singular directions, u_4 , u_5 , and u_6 are indicated in green, red, and blue respectively. In (a), the robot is in configuration $\theta = [0, 0, 0, 0, 0, 0, 0]$ and in (b) the robot is in $\theta = [\pi, 0, \pi, \pi, \pi, \pi, \pi]$.

Table 5: PA-10 robot's rank-3 singular configurations.

i	θ_1	θ_2	θ_3	θ_4	θ_5	θ_6	θ_7
1	x	$\pm\pi, 0$	$\pm\pi, 0$	$\pm\pi, 0$	$\pm\pi, 0$	$\pm\pi, 0$	x

can employ our technique to find any robot singular configuration but one must exclude infeasible angles due to mechanical limits.

4 CONCLUSIONS

This work has proposed a procedure based on computing the gradient of a singular value to drive a robot into a singular configuration. This algorithm is able to: (1) identify the singularities of any rank for any robot and (2) deal with ill-defined singular vectors when their corresponding singular values are equal. A second algorithm was presented to obtain the most intuitive representation of the singular vectors associated with configurations that correspond to high-rank singularities. Both algorithms are applicable to robots with an arbitrary number of degrees of freedom and of arbitrary kinematic structure. These algorithms were illustrated on a 4-DoF redundant positioning robot and on a 7-DoF redundant PA-10 robot.

REFERENCES

- Baker, D. R. and Wampler, C. W. (1988). On the inverse kinematics of redundant manipulators. *The International Journal of Robotics Research*, 7(2):3–21.
- Ben-Gharbia, K. M., Maciejewski, A. A., and Roberts, R. G. (2013). Kinematic design of redundant robotic manipulators for spatial positioning that are optimally fault tolerant. *IEEE Transactions on Robotics*, 29(5):1300–1307.
- Boudreau, R. and Podhorodeski, R. P. (2010). Singularity analysis of a kinematically simple class of 7-jointed revolute manipulators. *Transactions of the Canadian Society for Mechanical Engineering*, 34(1):105–117.
- Burdick, J. W. (1989). On the inverse kinematics of redundant manipulators: Characterization of the self-motion manifolds. *International Conference on Robotics and Automation*, 1(2):264–270.
- Corke, P. (2017). *Robotics, vision and control: Fundamental algorithms in MATLAB®*, volume 118. Springer.
- Groom, K. N., Maciejewski, A. A., and Balakrishnan, V. (1999). Real-time failure-tolerant control of kinematically redundant manipulators. *IEEE Transactions on Robotics and Automation*, 15(6):1109–1115.
- Hunt, K. H. (1986). Special configurations of robot-arms via screw theory. *Robotica*, 4(3):171–179.
- Kieffer, J. and Lenarcic, J. (1994). On the exploitation of mechanical advantage near robot singularities. *Informatica*, 18(3):315–323.
- Klein, C. A. and Chu, L.-C. (1997). Comparison of extended Jacobian and Lagrange multiplier based methods for resolving kinematic redundancy. *Journal of Intelligent & Robotic Systems*, 19(1):39–54.
- Litvin, F., Yi, Z., Castelli, V. P., and Innocenti, C. (1986). Singularities, configurations, and displacement functions for manipulators. *The International Journal of Robotics Research*, 5(2):52–65.
- Maciejewski, A. A. (1988). *The analysis and control of robotic manipulators operating at or near kinematically singular configurations*. PhD thesis, The Ohio State University.
- Nakamura, Y. and Hanafusa, H. (1986). Inverse kinematic solutions with singularity robustness for robot manipulator control. *Journal of Dynamic Systems, Measurement, and Control*, 108(3):163–171.
- Nokleby, S. B. and Podhorodeski, R. P. (2004a). Identifying multi-DOF-loss velocity degeneracies in kinematically-redundant manipulators. *Mechanism and Machine Theory*, 39(2):201–213.
- Nokleby, S. B. and Podhorodeski, R. P. (2004b). Identifying the 1-DOF-loss velocity-degenerate (singular) configurations of an 8-joint manipulator. *Transactions of the Canadian Society for Mechanical Engineering*, 28(2A):109–124.
- Sugimoto, K., Duffy, J., and Hunt, K. (1982). Special configurations of spatial mechanisms and robot arms. *Mechanism and Machine Theory*, 17(2):119–132.
- Waldron, K., Wang, S.-L., and Bolin, S. (1985). A study of the Jacobian matrix of serial manipulators. *Journal of Mechanisms, Transmissions, and Automation in Design*, 107(2):230–237.
- Xu, W., Zhang, J., Liang, B., and Li, B. (2016). Singularity analysis and avoidance for robot manipulators with nonspherical wrists. *IEEE Transactions on Industrial Electronics*, 63(1):277–290.
- Xu, W., Zhang, J., Qian, H., Chen, Y., and Xu, Y. (2013). Identifying the singularity conditions of Canadarm2 based on elementary Jacobian transformation. *2013 IEEE/RSJ International Conference on Intelligent Robots and Systems*, pages 795–800.